

# Accelerating AI and Computer Vision for Satellite Pose Estimation on the Intel Myriad X Embedded SoC

Vasileios Leon<sup>a</sup>, Panagiotis Minaidis<sup>a</sup>, George Lentaris<sup>b,a</sup>, Dimitrios Soudris<sup>a</sup>

<sup>a</sup>National Technical University of Athens, School of Electrical and Computer Engineering, Greece

<sup>b</sup>University of West Attica, Department of Informatics and Computer Engineering, Greece

## Abstract

The challenging deployment of Artificial Intelligence (AI) and Computer Vision (CV) algorithms at the edge pushes the community of embedded computing to examine heterogeneous System-on-Chips (SoCs). Such novel computing platforms provide increased diversity in interfaces, processors and storage, however, the efficient partitioning and mapping of AI/CV workloads still remains an open issue. In this context, the current paper develops a hybrid AI/CV system on Intel's Movidius Myriad X, which is an heterogeneous Vision Processing Unit (VPU), for initializing and tracking the satellite's pose in space missions. The space industry is among the communities examining alternative computing platforms to comply with the tight constraints of on-board data processing, while it is also striving to adopt functionalities from the AI domain. At algorithmic level, we rely on the ResNet-50-based UrsoNet network along with a custom classical CV pipeline. For efficient acceleration, we exploit the SoC's neural compute engine and 16 vector processors by combining multiple parallelization and low-level optimization techniques. The proposed single-chip, robust-estimation, and real-time solution delivers a throughput of up to 5 FPS for 1-MegaPixel RGB images within a limited power envelope of 2W.

**Keywords:** Heterogeneous Computing, Embedded System, System on Chip, Multi-Core Processor, VLIW Processor, Edge Device, Vision Processing Unit, Deep Neural Network, Computer Vision, Vision-Based Navigation, Pose Tracking, Space Avionics, COTS Component, Intel Myriad, OpenVINO, Neural Compute Engine.

## 1. Introduction

The rapid evolution of powerful Artificial Intelligence (AI) algorithms and sophisticated Computer Vision (CV) pipelines marks a new era of computing at the edge. The worldwide demand for high performance with a restricted power budget, especially when considering embedded systems, challenges the integration of AI/CV functionalities in novel applications. Heterogeneous System-on-Chip (SoC) processors emerge as a promising solution [1], providing increased programming flexibility and diversity in terms of processors and memories. A prominent class of heterogeneous SoCs is the Vision Processing Unit (VPU) [2, 3, 4], which excels in embedded low-power imaging applications, covering domains such as robotics, automotive, and space.

Space is one of the communities seeking alternative processing platforms to comply with the tight constraints of on-board processing. Towards this direction, the enhanced performance of modern edge devices can efficiently serve tasks for Earth Observation (EO) and Vision-Based Navigation (VBN). Satellite Pose Estimation [5, 6, 7, 8] constitutes a typical problem in such space applications, with its increased computing intensity stressing the conventional processors to provide sufficient throughput. Moreover, the heterogeneity of devices such

as the VPUs, allows for improved adaptability to various mission scenarios and seamless in-flight re-programmability. To further improve the Performance and Size-Weight-Power (SWaP), as well as additional costs (e.g., development effort), the space industry is studying mixed-criticality architectures [9, 10, 11, 12], i.e., the integration of both space-grade and Commercial-Off-The-Shelf (COTS) components. The use of COTS components in Low Earth Orbit (LEO) missions and CubeSats relies on the partial shielding provided by the Earth's magnetosphere and/or the short mission lifetime, which limit the damage or unavailability of electronics due to radiation. In this context, FPGAs [13, 14, 15, 16], GPUs [17, 18, 19, 20, 21] and VPUs [22, 23, 24, 25] are evaluated as accelerators, while COTS devices, e.g., Intel's Myriad 2 VPU, are subjected to radiation tests [26]. A second challenge for the space industry is the wider adoption of AI, which is currently limited to offline/ground data processing instead of on-board processing, mostly due to insufficient computational power and qualification issues when deployed in orbit [26].

In this paper, motivated by the aforementioned challenges in embedded computing and space avionics, we develop AI and CV functionalities for satellite pose estimation on Intel's 16-nm Myriad X VPU. Myriad X is the latest variant of Intel's VPU family, supporting custom and automatic AI deployment, as well as classic CV workloads. In particular, we accelerate a Deep Neural Network (DNN) of ResNet backbone, namely UrsoNet [5], which estimates the satellite's pose, next

\* Accepted for publication at *Elsevier Microprocessors and Microsystems*, Vol. 103, Nov. 2023, DOI: <https://doi.org/10.1016/j.micpro.2023.104947>

to a custom CV pipeline [6] tracking the pose. We select UrsoNet [5] and the CV of [6] because they are representative of high-performance state-of-the-art algorithms for the pose estimation/tracking problem. The two algorithmic pipelines are acting complementary to provide a single-chip solution to the entire pose estimation problem (initialization and tracking) and increase the robustness of the VBN subsystem. The experimental results show that the proposed low-level optimization and tuning improves the speedup provided by the default core parallelization. Overall, we perform pose estimation & tracking on 1-MegaPixel RGB images with a throughput of up to 5 FPS, while the power consumption of the SoC is around 2W. Moreover, we directly compare our implementations on the Myriad X VPU to other competitive embedded devices (CPUs, embedded GPUs, ARM-based FPGAs). The contribution of our work lies in two directions:

- (i) *Embedded Computing*: We propose a certain hybrid embedded system combining both AI and classic CV functions, while we accelerate them on an heterogeneous SoC by applying various low-level optimization techniques.
- (ii) *Space Avionics*: We propose a self-contained system for the entire relative pose estimation problem, i.e., Lost-In-Space and Tracking. Our solution is integrated in a single COTS SoC and provides excellent power consumption and sufficient performance. We evaluate a candidate device for on-board acceleration in mixed-criticality avionics architectures, while we examine practical AI functionalities for on-board processing (not widely adopted yet).

The remainder of this paper is organized as follows. Section 2 provides background in the use of COTS devices in space, while Section 3 introduces the Myriad VPU family. Section 4 introduces the proposed embedded AI/CV system, and it also discusses its mapping onto the Myriad X SoC and low-level implementation details. Section 5 reports and analyzes the experimental results, and finally, Section 6 draws the conclusions.

## 2. COTS Embedded Processors in Space

The literature includes a variety of COTS-based processing architectures and works evaluating the suitability of COTS devices for on-board use in future space missions. In this section, we report representative works for each type of COTS processor.

### 2.1. Field-Programmable Gate Arrays (FPGAs)

For high-performance solutions, COTS FPGAs are preferred, as they outperform both their space-grade counterparts [27] and the general-purpose CPUs [28]. The authors of [13] propose a runtime reconfigurable SW/HW on-board processor for VBN, which provides autonomous adaptation during the mission. The architecture relies on the RTEMS real-time operating system to apply reconfiguration and fault mitigation. The implementation is performed on Xilinx’s Zynq UltraScale+ MPSoC. The

Zynq-7000 SoC FPGA is used in [14] to implement compute-intensive CV algorithms for satellite pose tracking. This architecture is based on a HW/SW co-design methodology that exploits the full potential of the Zynq structure. Iturbe *et al.* [15] propose a HW/SW infrastructure for instrument data handling and processing, which is prototyped on Zynq-7000. They also equip their design with several hardening techniques for fault mitigation (e.g., watchdogs). The on-board space computer of [16], which is also based on the Zynq FPGA, integrates several functionalities towards improving in-flight reliability (e.g., memory scrubbing).

### 2.2. Graphics Processing Units (GPUs)

COTS embedded GPUs have also gained the interest of the space community. The GPU platforms can provide sufficient performance with less development effort than FPGAs. Kosmidis *et al.* [17] examine the applicability of mobile GPUs in the space domain, covering both the software and hardware perspectives. In particular, they analyze the algorithms and workloads of space applications to identify their suitability for GPUs, and they also perform a benchmarking evaluation on GPUs. In [18], the authors evaluate two graphics-based computing methodologies (OpenGL 2.0 and Brook Auto) for safety-critical systems. Their benchmark is an application modeling a VBN scenario in which the aircraft performs rendez-vous with an object. Moreover, the literature includes FPGA-GPU co-processing architectures. The hybrid FPGA-GPU architecture of [19] employs Nvidia’s Tegra X2/X2i GPU as main accelerator. The heterogeneous architecture of [20] integrates a SoC FPGA for SpaceWire I/O transcoding, the AMD SoC (CPU & GPU) for acceleration, and optionally, a VPU for AI deployment. The authors of [29] deploy neural networks for object detection along with image compression techniques on Nvidia’s Jetson Nano GPU. More recently, in [21], embedded GPU platforms are evaluated for accelerating data compression standards for space applications.

### 2.3. Vision Processing Units (VPUs)

The Intel’s Myriad family of VPUs is systematically being evaluated by the space community. In [26], Furano *et al.* report results from the radiation testing of Myriad 2, which involves different functional tests and characterization of all SoC’s memories. According to their experiments, Myriad 2 remains fully functional after exposed to a total ionizing dose of 49 krad(Si). The same VPU is used to accelerate CV algorithms for VBN applications [22], and specifically, it provides a throughput of up to 5 FPS for pose estimation on 1-MegaPixel images within the power envelope of 1W. Agarwal *et al.* [30] evaluate Myriad 2 for implementing a star identification neural network. The results show that Myriad 2 provides sufficient performance, while consuming around 1W and retaining an accuracy of 99.08%. Moreover, Myriad 2 is equipped on-board in the  $\Phi$ -Sat-1 CubeSat mission of the European Space Agency as DNN demonstrator for EO [23, 31]. Myriad 2 is also placed in custom boards for use in space. In particular, Ubotica’s CogniSAT CubeSat board [32] is an AI inference and CV engine that exposes the compute of Myriad 2 to the payload developer. In

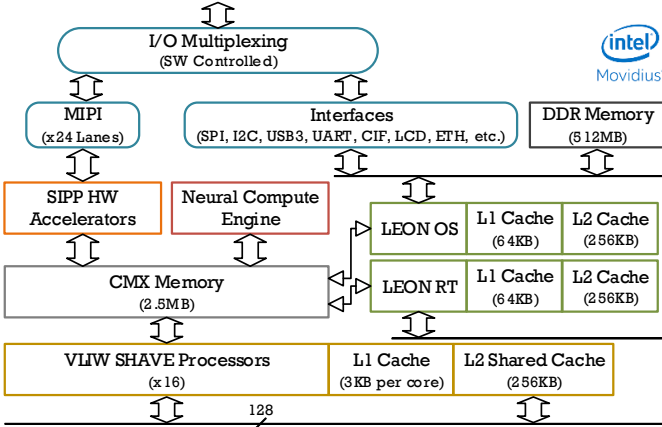


Figure 1: Intel's Myriad X VPU [4].

the same context, Myriad 2 is integrated as the main accelerator in the HPCB platform [24], which is a payload data processor board for mixed-criticality space avionics. The results show that Myriad 2 can provide sufficient AI acceleration with limited power consumption, while it sustains remarkable I/O throughput [25]. To increase the reliability of Myriad 2 as part of a mixed-criticality architecture, the authors of [33] propose fault-tolerant techniques tailored to this SoC. Myriad X, which is the newest VPU and the successor of Myriad 2, has received less attention. In [34], the authors report results for deploying neural networks classifiers on Myriad X. The networks are trained on Mars imagery from the Reconnaissance Orbiter and Curiosity rover, and the average inference time is 16-20ms with power lying around 1.8-1.9W.

### 3. The Myriad Vision Processing Unit

The Myriad family of VPUs includes multi-core COTS SoCs that target to terrestrial mobile and embedded applications [2, 3]. The SoCs integrate multiple peripherals for I/O, hardware filters for low-power image processing, and general-purpose & vector processors. All these components are connected to a multi-ported high-bandwidth shared memory hierarchy. The heterogeneity of Myriad VPUs allows for efficient mapping of AI and CV algorithms with a power of 1-2W (depending on the VPU variant). Besides their usage in space, the Myriad VPUs are employed for implementing DNNs [35, 36, 37, 38], machine learning algorithms (e.g., SVM classifiers [39]), and CV functions (e.g., stereo vision [40]).

In this work, we employ the Myriad X VPU, which is illustrated in Fig. 1. Contrary to Myriad 2, this variant features a dedicated on-chip accelerator, called Neural Computer Engine (NCE), for inferencing DNNs. It also integrates 16 programmable 128-bit VLIW vector cores (called SHAVES) for accelerating CV functions, hardware accelerators for imaging/vision tasks, and 2 general-purpose LEON4 processors (called LEON OS and LEON RT). Regarding the memory hierarchy, Myriad X provides on-chip 512MB LPDDR4 DRAM, 2.5MB scratchpad memory (called CMX), as well caches for LEONs and SHAVES. Furthermore, the SoC offers numerous imaging

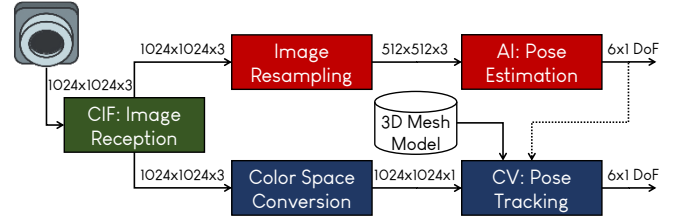


Figure 2: Cooperation of AI and CV for pose estimation/tracking on Myriad X.

(MIPI lanes, CIF, LCD) and general-purpose (e.g., SPI, USB, UART) I/O interfaces.

The Myriad X SoC is programmed via the Myriad Development Kit (MDK), which includes all the necessary tools (e.g., toolchain for the processors, C/C++ compiler, debugger) to implement custom CV and DNN algorithms. To deploy DNNs of well-known frameworks (e.g., TensorFlow) on NCE, the Intel's OpenVINO toolkit [41] is used. OpenVINO takes the frozen graph as input and employs tools such as the model optimizer and the Myriad compiler to generate the programming file. This binary network file is loaded on NCE via the mvNCI API, which is also used to feed NCE with input data and receive its outputs in the form of tensors.

## 4. AI/CV Acceleration for Lost-In-Space on Myriad X

The targeted AI/CV system for pose estimation & tracking is illustrated in Fig. 2. The input image is received by the Camera InterFace (CIF) of the VPU [25], it is stored in DRAM, and then it is subjected to pre-processing. For the AI pipeline (upper block), the pre-processing applies resampling to reduce the image resolution, and thus facilitate DNN inferencing at the edge. Our DNN is a mobile version of the UrsoNet network [5], satisfying the real-time processing constraints. For the CV pipeline (lower block), the pre-processing converts the image to grayscale, as required by our 5-stage CV algorithm [6, 22].

The purpose of the current work is to quantify the costs and benefits of the two complementary algorithmic pipelines (CV and AI), fine-tune their implementation on Myriad X, and evaluate the potential gains of their acceleration on a single low-power SoC. We note that the final system integration would also include a high-level policy mechanism to coordinate the two pipelines, e.g., (i) decide when to provide an initial pose via AI and when to continue tracking via CV, or (ii) execute both pipelines for the same input and decide which pose to keep; the creation of such a policy mechanism requires additional exploration with test campaigns and customization to real satellite datasets (e.g., to identify when the pose is lost).

### 4.1. Pre-Processing

To explore different trade-offs between DNN's performance and accuracy, we employ three well-established resampling algorithms with increasing computational complexity. First, Bilinear Interpolation inputs  $2 \times 2$  pixel regions with a stride equal to the reciprocal of the scaling factor and calculates the mean value per region. Second, Bicubic Interpolation inputs  $4 \times 4$

pixel regions and applies a cubic polynomial per region. Finally, Lanczos Interpolation reconstructs the pixels through a Lanczos kernel (windowed sinc function), and then applies interpolation using convolution; in this work, we consider  $8 \times 8$  pixel regions.

The image resampling algorithms are accelerated on SHAVES, while LEON OS monitors the execution and performs tasks such as initializing the SHAVES and passing the entry points to them. At system level, we configure the RTEMS Real-Time Operating System (RTOS) for LEON, define the memory space of DRAM and CMX, and set the clock of the SoC at the maximum frequency (700MHz). In terms of high-level design, the input image is divided into stripes, i.e., segments of successive image rows, and LEON OS assigns one stripe to each SHAVE to enable *core parallelization*. The input image is stored in DRAM (global memory), and each SHAVE transfers its own stripe in a dedicated slice of CMX (scratchpad memory) via the SoC’s DMA engine.

Regarding low-level development details, the resampling algorithms are implemented in an iterative manner on SHAVES. In particular, each SHAVE performs a call to the selected resampling function per loop iteration, producing the output rows of its assigned image stripe one by one. Therefore, the number of image rows required to be transferred to each SHAVE’s CMX slice per loop iteration is equal to the height of the algorithm’s resampling region (e.g., 4 for Bicubic). Considering a scaling factor of 0.5 (i.e., stride equal to 2), each loop iteration of Bicubic ( $4 \times 4$  region) and Lanczos ( $8 \times 8$  region) needs to fetch only two new image rows. To take advantage of this property, we employ a data structure that implements a double-linked list, where each node contains a row buffer, and thus, *sliding buffer* is enabled by re-arranging the pointers that connect the nodes. We also exploit the SoC’s support for numerous data types (e.g., “u8”, “u16”, and “float16”) to apply *variable tuning*. Moreover, we enable *SIMD computations* by arranging the data into 128-bit vectors and calling the corresponding routines to deploy additions and dot products on SoC’s scalar arithmetic unit. The compiler is also enabled to map arithmetic operations onto the vector arithmetic unit.

#### 4.2. Deep Neural Network for Pose Estimation

We employ the UrsoNet DNN [5] for estimating the satellite’s pose. The architecture of UrsoNet, which is based on the ResNet-50 network, is illustrated in Fig. 3. In comparison with the original ResNet architecture, the global average pooling layer and last fully-connected layer are removed. In their place, the designers of UrsoNet [5] insert a bottleneck layer consisting of a  $3 \times 3$  convolution with stride 2 as well as two fully-connected layers calculating the satellite’s location and orientation. To build our network, we use the “soyuz\_hard” dataset and follow the training guidelines of [5]. The dataset is split using an 80-10-10 scheme, that is, 4000 images comprise the training set, while the validation and testing set consist of 500 of the remaining images each. The configuration of UrsoNet for deploying it on Myriad X is reported in Table 1. The initial weights of the backbone are acquired from a Mask R-CNN model pre-trained on the COCO dataset, as suggested

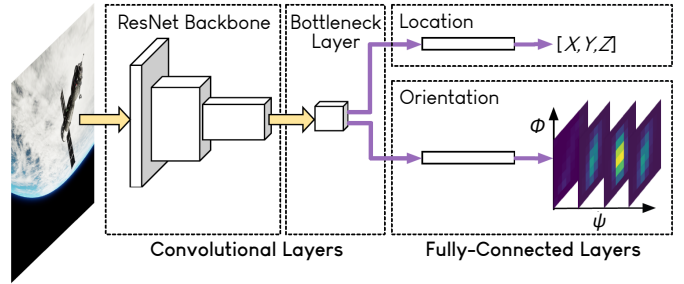


Figure 3: The architecture of the UrsoNet DNN for pose estimation [5].

Table 1: The configuration of the UrsoNet DNN for deployment on Myriad X

Backbone	ResNet-50
Bottleneck Width	128
Branch Size	512
Input Image	$1024 \times 1024 \times 3$
Resampling	Bilinear, Bicubic, Lanczos
Inference Image	$512 \times 512 \times 3$
Ori./Loc. Resolution	16/16
Pre-Trained Weights	COCO
Dataset	“soyuz_hard”
Arithmetic	16-bit floating-point
Epochs	100
Image Augmentation	Yes
Optimizer	SGD

in [5]. Data augmentation is performed by randomly rotating half of the training images per epoch. The image resolution is decreased using the resampling algorithms and zero padding. All models are trained for 100 epochs on Nvidia’s Tesla V100 GPU.

To generate the binary network file and deploy it on the USB NCS2 accelerator of Myriad X, we follow the typical OpenVINO toolflow [41]. Fig. 4 illustrates the mapping of the basic network blocks of our UrsoNet architecture on Myriad X. Compared to the original ResNet architecture, the batch normalization blocks are replaced by add operations, which are accelerated on SHAVES. Smaller operations, e.g., some permutations before the fully-connected layers, are also executed on SHAVES. The convolutions and fully-connected layers are mapped onto NCE, while almost all the ReLU activation functions are optimized out by OpenVINO during the graph transformation stage, i.e., they are fused with other operations.

#### 4.3. Computer Vision Pipeline for Pose Tracking

The continuous tracking of the satellite’s pose is performed with a classic CV pipeline [6, 22], which is illustrated in Fig. 5. This algorithmic pipeline involves functions for feature detection, perpendicular matching, image/depth rendering, and linear algebra operations. In particular, the pipeline evolves an initial pose by matching edges detected on the input image and a depth map (rendered from the satellite’s 3D mesh model). The matching edges are then used to refine the 6D pose via robust regression calculations. For the Edge Detection function, we employ the well-established Canny edge detector [42], which



Table 2: Experimental results for the pose estimation AI pipeline on Myriad X (1024×1024×3 input image resampled to 512×512×3 for DNN inference)

Algorithm	Image Resampling							DNN Inference <sup>4</sup>				AI: Pose Estimation	
	Performance			Power				Performance		Accuracy		Performance	
	Latency	Improv. <sup>1</sup>	Speedup <sup>2</sup>	Core	DRAM	Total	Improv. <sup>3</sup>	Latency	Speedup <sup>5</sup>	LOCE <sup>6</sup>	ORIE <sup>6</sup>	Latency	Throughput
Bilinear	1ms	141×	425×	1.9W	0.1W	2.0W	10%	373ms	5×	1.18m	14.76°	374ms	2.7 FPS
Bicubic	6ms	68×	285×	1.9W	0.1W	2.0W	9%	373ms	5×	1.15m	14.62°	379ms	2.6 FPS
Lanczos	19ms	55×	360×	2.1W	0.1W	2.2W	9%	373ms	5×	1.15m	14.57°	392ms	2.6 FPS

<sup>1</sup> improvement vs. straightforward SHAVE parallelization<sup>3</sup> improvement vs. default power management<sup>5</sup> speedup vs. original DNN (1024×1024×3 image)<sup>2</sup> speedup vs. execution on LEON4 CPU<sup>4</sup> synchronous inference (throughput = 1/latency)<sup>6</sup> LOCE=1.3m & ORIE=10.7° in original DNN without resampling [5]

5–8 of Table 2). Our resampled DNN inference on NCE & SHAVes is evaluated by comparing it with the respective execution on the same processors for the original 1-MegaPixel image (columns 9–12 of Table 2). Finally, we examine the performance of the entire AI pipeline (columns 13–14 of Table 2). Regarding the CV pipeline, we evaluate its acceleration on the SHAVes of Myriad X in comparison with the respective optimized implementation on Myriad 2 and the execution on the LEON4 CPU of Myriad 2 (columns 3–4 of Table 3).

## 5.2. Experimental Results on Myriad X VPU

Table 2 reports our results per AI pipeline and resampling algorithm. The focus is on performance (i.e., speed) and power. The latency of the pre-processing stage is 1–20ms, depending on the algorithm, which implies 55–141× performance improvement versus the straightforward parallelization on SHAVes without the optimizations (sliding buffer, variable tuning, SIMD) and the use of the scratchpad memory (CMX). Compared to LEON4, the speedup is remarkable, i.e., up to 425×. In terms of power, our manager improves the consumption by 10%, delivering around 2W (95% of the total power is consumed by the LEON4 and SHAVE processors). Moreover, a single DNN inference (synchronous execution) on a 512×512×3 image requires around 373ms, which is 5× faster than inferencing on the initial 1-MegaPixel image. At the same time, the mean Location Error (LOCE) is 1.15–1.18m and the mean Orientation Error (ORIE) is 14.57°–14.76° for the “soyuz\_hard” dataset, i.e., both accuracy metrics are in the range of the respective values reported in [5]. As a result, like in [5], the accuracy of our DNN is close to that of the DNN without resampling (LOCE is 1.3m and ORIE is 10.7°). Furthermore, the network trained with the same configuration on the “soyuz\_easy” dataset has a LOCE equal to 0.7m and an ORIE of 8.7°. These values are sufficiently close to the results reported in [5], namely 0.6m LOCE and 8.0° ORIE, however, once again the average latency is retained at 373ms, indicating that training does not impact the performance. In all cases, more fine-grained training can provide better accuracy results for the same performance on the Myriad X SoC. Overall, the entire AI pipeline achieves 2.6–2.7 FPS for synchronous execution (throughput will increase for asynchronous inferencing).

From the CV pipeline, Depth Rendering is the most demanding function, providing a variable latency as it is highly dependent on the image content. Our techniques (dynamic scheduling, SIMD and cache optimization) improve the latency of this

Table 3: Performance of the pose tracking CV pipeline on Myriad X

Function	Latency	Speedup <sup>1</sup>	Speedup <sup>2</sup>
Intensity Edge Detection	24ms	15×	1.5×
Depth Rendering	77–170ms	20×	1.5×
Depth Edge Detection	26ms	15×	1.5×
Edge Matching	1ms	100×	5×
Pose Refinement	90–120ms	1.1×	1.1×
<b>CV: Pose Tracking</b>	218–341ms <sup>3</sup>	13×	1.4×

<sup>1</sup> speedup vs. LEON4 @600MHz (Myriad 2)<sup>2</sup> speedup vs. 12 SHAVes @600MHz (Myriad 2)<sup>3</sup> sequential execution (without the scheduling of Fig. 6)

Table 4: Performance of Lost-In-Space modules on Myriad X

Module	Input Data	Latency	Throughput
CIF: Image Reception <sup>1</sup>	1024×1024×3	63ms	16 FPS
Pre-Processing	1024×1024×3	1–19ms	50–1000 FPS
AI: Pose Estimation	512×512×3	373ms	2.7 FPS
CV: Pose Tracking	1024×1024×1	218–341ms	3.1–5.1 FPS <sup>2</sup>

<sup>1</sup> CIF@50MHz<sup>2</sup> with function masking for streaming processing (scheduling, Fig. 6)

function by 8× compared to the straightforward parallelization on SHAVes. Similar improvements are also delivered in the Edge Detection function. Edge Matching is a memory-intensive function involving comparisons, thus, it is facilitated by our cache optimizations to deliver a speedup of 4× compared to the straightforward SHAVE parallelization. In Table 3, we report the latency results for the CV pipeline along with the gains compared to the LEON4 and SHAVE processors of Myriad 2 [22]. Compared to LEON4, the speedup is 15–20× for the compute-intensive functions and 100× for the memory-intensive function. Furthermore, compared to the SHAVE implementation on Myriad 2, we notice a speedup of 1.5× and 5×, respectively, which mainly comes from the 4 extra SHAVes (16 in Myriad X) and the increased clock frequency (700MHz in Myriad X). Finally, in terms of accuracy, the error is below 0.5m and tracking is lost only in a few frames.

Table 4 summarizes the performance of each module of the targeted AI/CV embedded system. The image reception via CIF operating at 50MHz lasts 63ms according to our experiments with an FPGA transmitting data to the VPU [25]. The pre-processing time is negligible compared to the AI/CV execution, which sustains a throughput of 2.7–5.1 FPS (sufficient for pose estimation on 1-MegaPixel images). We note that fur-

Table 5: Performance of embedded processors for the UrsoNet DNN (TensorFlow, inference on  $512 \times 640 \times 3$  image)

Device	Processor	Latency	Throughput	Power	Throughput-per-Watt
Intel Myriad X VPU (NCS2)	NCE + 16-core SHAVE @700MHz	588ms	1.7 FPS	5W <sup>1</sup>	0.34 FPS
ARM Cortex-A57 CPU (Jetson Nano)	4-core @1.4GHz	2830ms	0.4 FPS	10W	0.04 FPS
	2-core @918MHz	7519ms	0.1 FPS	5W	0.02 FPS
Nvidia Maxwell GPU (Jetson Nano)	128-core @921MHz	761ms	1.3 FPS	10W	0.13 FPS
	128-core @614MHz	958ms	1 FPS	5W	0.2 FPS

<sup>1</sup> NCS2 (2W) hosted on Raspberry Pi 3 (3W).

ther speedups can be achieved, e.g., inferencing on  $192 \times 256 \times 3$  image delivers 15 FPS with reasonable accuracy loss (LOCE is 1.9–2m), while the throughput of the CV pipeline can be improved by rendering a smaller image.

### 5.3. Comparison to Embedded Devices

In this section, we provide comparisons to other embedded devices that are also considered for space avionics. In particular, we compare our implementations on Myriad X with the execution on CPUs (LEON, ARM), GPUs (Jetson Nano, Tegra K1), and SoC FPGAs (Zynq).

Starting with UrsoNet, Table 5 presents the results for inferencing on VPU, CPU, and GPU. For this experiment, we use input images that are scaled to  $512 \times 640 \times 3$  size. The CPU is the ARM Cortex-A57 of Nvidia’s Jetson Nano board, while our GPU is the 128-core Maxwell of the same board. For Jetson Nano, we consider its two power modes: the “low-power” at 5W and the “high-performance” at 10W. To make a fair comparison, we consider the NCS2 VPU hosted on a single board computer, i.e., a Raspberry Pi 3, and thus, the total power consumption for inferencing is 5W. In terms of latency, the 4-core Cortex-A57 operating at 1.4GHz is relatively slow, i.e., NCS2 achieves a  $6 \times$  speedup. Compared to the GPU, NCS2 achieves a slight improvement of  $1.3 \times$ , but with half of the GPU’s power consumption. When considering both throughput and power, NCS2 delivers  $\sim 1.7 \times$  more FPS per Watt than GPU and  $\sim 8.5 \times$  more FPS per Watt than CPU. In addition, we provide comparison results for the original ResNet-50 network ( $224 \times 224 \times 3$  image), which is the backbone of UrsoNet. For this network, the Jetson Nano GPU provides increased throughput versus Pi 3 + NCS2, i.e.,  $1.3\text{--}1.9 \times$  more FPS, however, when considering FPS-per-Watt, the VPU inference outperforms the GPU by  $1.1\text{--}1.5 \times$ . Finally, we note that if we use the Myriad X SoC rather than the pair Pi 3 + NCS2, the proposed solution provides even better results against the competitor devices. In this case, the power consumption lies around 2–2.5W, while the latency does not include the USB communication time ( $\sim 10$ ms).

Next, we evaluate the acceleration of our CV functions compared to implementations on other embedded devices. Table 6 summarizes the comparison with other works of the literature implementing the same functions. As already discussed in the previous subsection, Myriad X outperforms its predecessor Myriad 2 by  $\sim 1.5 \times$ , while compared to the general-purpose LEON4 CPU, it provides acceleration of  $15\text{--}20 \times$  for the most demanding functions. Compared to ARM Cortex-A9 of Xilinx’s Zynq [14], we achieve remarkable speedup, i.e.,  $\sim 14 \times$

Table 6: Improvements by our CV implementations versus literature works

Design	Device	Improvement	Ref.
CV Functions	Myriad 2	$\sim 1.5 \times$ speedup	[22]
CV Functions	LEON4	$\sim 15\text{--}20 \times$ speedup	[22]
Edge Detection	ARM Cortex-A9	$14 \times$ speedup	[14]
Depth Rendering	ARM Cortex-A9	$10 \times$ speedup	[14]
Edge Matching	ARM Cortex-A9	$39 \times$ speedup	[14]
Edge Detection	Tegra K1	$3 \times$ performance-per-Watt	[43]
CV Pipeline	Zynq-7000	$3.5\text{--}4 \times$ better power	[14]
CV Pipeline	Zynq-7000	$1.4 \times$ performance-per-Watt	[14]

for Canny Edge Detection (326ms on Cortex-A9),  $\sim 10 \times$  for Depth Rendering (869ms on Cortex-A9), and  $39 \times$  for Edge Matching (39m on Cortex-A9). Compared to Nvidia’s Tegra K1 GPU [43], Myriad X provides  $2 \times$  worse latency for Canny Edge Detection (12ms on Tegra K1 for 1-MegaPixel images). However, in terms of performance-per-Watt, Myriad X is  $3 \times$  better than Tegra K1 consuming 10W.

Finally, we compare our CV implementation on Myriad X to that on the programmable logic of Zynq-7000 [14]. The results show that Myriad X trades off speed for power, i.e., it is  $2.5\text{--}3 \times$  slower than the FPGA (considering the entire CV pipeline), however, it is  $3.5\text{--}4 \times$  better in terms of mean power consumption. Furthermore, it exhibits stable power consumption (2W) compared to the FPGA, which has a variation between 2W and 9W. Besides better power and performance per Watt, the Myriad X provides additional benefits versus the FPGA. First, the large DDR memory of Myriad X can facilitate in-flight programmability in space avionics, i.e., store different algorithms/applications that can be seamlessly programmed. On the other hand, the FPGA requires the development of dynamic re-configuration techniques, which also add timing penalties. Second, to support AI acceleration and fast DNN deployment on Zynq, the developer has to build Xilinx’s Deep Learning Processor Unit (DPU). Therefore, considering the resources required for the DPU, a device like Zynq-7000 is stressed to implement the entire system (UrsoNet DNN + CV pipeline), as the CV kernel already utilizes increased resources, i.e., 36% LUTs, 48% DSPs, and 77% RAMBs [14].

## 6. Conclusion and Future Work

The paper showed that heterogeneous embedded SoCs integrating diverse processors (general-purpose, vector, neural) can provide promising AI/CV solutions in challenging prob-

lems for space, such as pose estimation in lost-in-space and satellite tracking scenarios. We combined low-level optimizations, evaluated the capabilities of Myriad X, and quantified the total costs of each algorithm in the targeted AI/CV system. The results showed that the Myriad X VPU directly competes with other state-of-the-art processors, widely considered for space applications, offering promising throughput and significantly lower power consumption. Our future work includes improving the cooperation between the AI and CV pipelines by customizing on certain datasets/sequences and fine-tuning the high-level SW mechanism to switch between pipelines in real time.

## Acknowledgement

The authors would like to thank M. Lourakis & X. Zabulis for providing the initial software of the CV pipeline, and P. Proença & Y. Gao for providing the UrsoNet code in GitHub.

## References

- [1] S. Mittal, J. S. Vetter, A survey of CPU-GPU heterogeneous computing techniques, *ACM Computing Surveys* 47 (4) (2015) 1–35. doi:10.1145/2788396.
- [2] B. Barry, C. Brick, F. Connor, D. Donohoe, D. Moloney, R. Richmond, M. O’Riordan, V. Toma, Always-on vision processing unit for mobile applications, *IEEE Micro* 35 (2) (2015) 56–66. doi:10.1109/MM.2015.10.
- [3] D. Moloney, B. Barry, R. Richmond, F. Connor, C. Brick, D. Donohoe, Myriad 2: Eye of the computational vision storm, in: *IEEE Hot Chips Symposium (HCS)*, 2014, pp. 1–18. doi:10.1109/HOTCHIPS.2014.7478823.
- [4] E. Petrongonas, V. Leon, G. Lentaris, D. Soudris, ParalOS: A scheduling & memory management framework for heterogeneous VPUs, in: *Euromicro Conference on Digital System Design (DSD)*, 2021, pp. 221–228. doi:10.1109/DSD53832.2021.00043.
- [5] P. F. Proença, Y. Gao, Deep learning for spacecraft pose estimation from photorealistic rendering, in: *IEEE International Conference on Robotics and Automation (ICRA)*, 2020, pp. 6007–6013. doi:10.1109/ICRA40945.2020.9197244.
- [6] M. Lourakis, X. Zabulis, Model-based visual tracking of orbiting satellites using edges, in: *IEEE/RSJ International Conference on Intelligent Robots and Systems (IROS)*, 2017, pp. 3791–3796. doi:10.1109/IROS.2017.8206228.
- [7] P. Carcagni, M. Leo, P. Spagnolo, P. L. Mazzeo, C. Distante, A lightweight model for satellite pose estimation, in: *International Conference on Image Analysis and Processing (ICIAP)*, 2022, p. 3–14. doi:10.1007/978-3-031-06427-2\_1.
- [8] Y. Hu, S. Speierer, W. Jakob, P. Fua, M. Salzmann, Wide-depth-range 6D object pose estimation in space, in: *IEEE/CVF Conference on Computer Vision and Pattern Recognition (CVPR)*, 2021, pp. 15865–15874. doi:10.1109/CVPR46437.2021.01561.
- [9] A. D. George, C. M. Wilson, Onboard processing with hybrid and reconfigurable computing on small satellites, *Proceedings of the IEEE* 106 (3) (2018) 458–470. doi:10.1109/JPROC.2018.2802438.
- [10] A. Crespo, A. Alonso, M. Marcos, J. A. de la Puente, P. Balbastre, Mixed criticality in control systems, *IFAC Proceedings Volumes* 47 (3) (2014) 12261–12271. doi:10.3182/20140824-6-ZA-1003.02004.
- [11] S. Esposito, M. Violante, System-level architecture for mixed criticality applications on MPSoC: A space application, in: *IEEE International Workshop on Metrology for AeroSpace (MetroAeroSpace)*, 2017, pp. 479–483. doi:10.1109/MetroAeroSpace.2017.7999621.
- [12] V. Leon, G. Lentaris, D. Soudris, S. Vellas, M. Bernou, Towards employing FPGA and ASIP acceleration to enable onboard AI/ML in space applications, in: *IFIP/IEEE International Conference on Very Large Scale Integration (VLSI-SoC)*, 2022, pp. 1–4. doi:10.1109/VLSI-SoC54400.2022.9939566.
- [13] A. Pérez, A. Rodríguez, A. Otero, D. González-Arjona, A. Jiménez-Peralo, M. A. Verdugo, E. De La Torre, Run-time reconfigurable MPSoC-based on-board processor for vision-based space navigation, *IEEE Access* 8 (2020) 59891–59905. doi:10.1109/ACCESS.2020.2983308.
- [14] G. Lentaris, I. Stratakos, I. Stamoulias, D. Soudris, M. Lourakis, X. Zabulis, High-performance vision-based navigation on SoC FPGA for spacecraft proximity operations, *IEEE Transactions on Circuits and Systems for Video Technology* 30 (4) (2020) 1188–1202. doi:10.1109/TCSVT.2019.2900802.
- [15] X. Iturbe, D. Keymeulen, E. Ozer, P. Yiu, D. Berisford, K. Hand, R. Carlson, An integrated SoC for science data processing in next-generation space flight instruments avionics, in: *IFIP/IEEE International Conference on Very Large Scale Integration (VLSI-SoC)*, 2015, pp. 134–141. doi:10.1109/VLSI-SoC.2015.7314405.
- [16] D. Rudolph, C. M. Wilson, J. Stewart, P. Gauvin, A. D. George, H. Lam, G. Crum, M. J. Wirthlin, A. Wilson, A. Stoddard, CSP: A multifaceted hybrid architecture for space computing, in: *AIAA/USU Conference on Small Satellites*, 2014, pp. 1–7.
- [17] L. Kosmidis, I. Rodriguez, Álvaro Jover, S. Alcaide, J. Lachaize, J. Abella, O. Notebaert, F. J. Cazorla, D. Steenari, GPU4S: Embedded GPUs in space - latest project updates, *Elsevier Microprocessors and Microsystems* 77 (2020) 1–10. doi:10.1016/j.micpro.2020.103143.
- [18] M. Benito, M. M. Trompouki, L. Kosmidis, J. D. Garcia, S. Carretero, K. Wenger, Comparison of GPU computing methodologies for safety-critical systems: An avionics case study, in: *Design, Automation & Test in Europe (DATE)*, 2021, pp. 717–718. doi:10.23919/DATE51398.2021.9474060.
- [19] C. Adams, A. Spain, J. Parker, M. Hevert, J. Roach, D. Cotten, Towards an integrated GPU accelerated SoC as a flight computer for small satellites, in: *IEEE Aerospace Conference*, 2019, pp. 1–7. doi:10.1109/AERO.2019.8741765.
- [20] F. C. Bruhn, N. Tsog, F. Kunkel, O. Flordal, I. Troxel, Enabling radiation tolerant heterogeneous GPU-based onboard data processing in space, *CEAS Space Journal* 12 (2020) 551–564. doi:10.1007/s12567-020-00321-9.
- [21] A. Jover-Alvarez, I. Rodriguez, L. Kosmidis, D. Steenari, Space compression algorithms acceleration on embedded multi-core and GPU platforms, *ACM SIGAda Ada Letters* 42 (1) (2022) 100–104. doi:10.1145/3577949.3577969.
- [22] V. Leon, G. Lentaris, E. Petrongonas, D. Soudris, G. Furano, A. Tavoularis, D. Moloney, Improving performance-power-programmability in space avionics with edge devices: VBN on Myriad2 SoC, *ACM Transactions on Embedded Computing Systems* 20 (3) (2021) 1–23. doi:10.1145/3440885.
- [23] G. Giuffrida, L. Fanucci, G. Meoni, M. Batič, L. Buckley, A. Dunne, C. Van Dijk, M. Esposito, J. Hefele, N. Vercruyssen, G. Furano, M. Pastena, J. Aschbacher, The  $\Phi$ -Sat-1 mission: the first on-board deep neural network demonstrator for satellite earth observation, *IEEE Transactions on Geoscience and Remote Sensing* 60 (2022) 1–14. doi:10.1109/TGRS.2021.3125567.
- [24] J. E. Navarro, A. Samuelsson, H. Gingsjö, J. Barendt, A. Dunne, L. Buckley, D. Reisis, A. Kyriakos, E.-A. Papatheofanous, C. Bezaitis, P. Matthijs, J. P. Ramos, D. Steenari, High-performance compute board – a fault-tolerant module for on-board vision processing, in: *European Workshop on On-Board Data Processing (OBDP)*, 2021, pp. 1–7. doi:10.5281/zenodo.5521624.
- [25] V. Leon, C. Bezaitis, G. Lentaris, D. Soudris, D. Reisis, E.-A. Papatheofanous, A. Kyriakos, A. Dunne, A. Samuelsson, D. Steenari, FPGA & VPU co-processing in space applications: Development and testing with DSP/AI benchmarks, in: *IEEE International Conference on Electronics, Circuits and Systems (ICECS)*, 2021, pp. 1–5. doi:10.1109/ICECS53924.2021.9665462.
- [26] G. Furano, G. Meoni, A. Dunne, D. Moloney, V. Ferlet-Cavrois, A. Tavoularis, J. Byrne, L. Buckley, M. Psarakis, K.-O. Voss, L. Fanucci, Towards the use of Artificial Intelligence on the edge in space systems: Challenges and opportunities, *IEEE Aerospace and Electronic Systems Magazine* 35 (12) (2020) 44–56. doi:10.1109/MAES.2020.3008468.
- [27] V. Leon, I. Stamoulias, G. Lentaris, D. Soudris, D. Gonzalez-Arjona, R. Domingo, D. M. Codinachs, I. Conway, Development and testing on

- the European space-grade BRAVE FPGAs: Evaluation of NG-Large using high-performance dsp benchmarks, *IEEE Access* 9 (2021) 131877–131892. doi:10.1109/ACCESS.2021.3114502.
- [28] G. Lentaris, K. Maragos, I. Stratakos, L. Papadopoulos, O. Papanikolaou, D. Soudris, M. Lourakis, X. Zabulis, D. Gonzalez-Arjona, G. Furano, High-performance embedded computing in space: Evaluation of platforms for vision-based navigation, *Journal of Aerospace Information Systems* 15 (4) (2018) 178–192. doi:10.2514/1.I010555.
- [29] M. Lofqvist, J. Cano, Accelerating deep learning applications in space, in: *AIAA/USU Conference on Small Satellites*, 2020, pp. 1–19.
- [30] S. Agarwal, E. Hervas-Martin, J. Byrne, A. Dunne, J. Luis Espinosa-Aranda, D. Rijlaarsdam, An evaluation of low-cost vision processors for efficient star identification, *MDPI Sensors* 20 (21) (2020) 1–14. doi:10.3390/s20216250.
- [31] L. Buckley, A. Dunne, G. Furano, M. Tali, Radiation test and in orbit performance of MPSoC AI accelerator, in: *IEEE Aerospace Conference (AERO)*, 2022, pp. 1–9. doi:10.1109/AERO53065.2022.9843440.
- [32] A. Dunne, UB0100 AI & CV compute engine, in: *ESA Workshop on Avionics, Data, Control and Software Systems (ADCSS)*, 2020, pp. 1–17.
- [33] V. Leon, E. A. Papatheofanous, G. Lentaris, C. Bezaitis, N. Mastorakis, G. Bampilis, D. Reisis, D. Soudris, Combining fault tolerance techniques and COTS SoC accelerators for payload processing in space, in: *IFIP/IEEE International Conference on Very Large Scale Integration (VLSI-SoC)*, 2022, pp. 1–6. doi:10.1109/VLSI-SoC54400.2022.9939621.
- [34] E. Dunkel, J. L. Espinosa-Aranda, J. Romero-Canas, L. Buckley, Z. Towfic, F. Mirza, J. Swope, D. Russell, J. Sauvageau, D. Sheldon, S. Chien, M. Fernandez, C. Knox, K. Wagstaff, S. Lu, M. Denbina, D. Atha, M. Swan, M. Ono, Benchmarking machine learning on the Myriad X processor onboard the ISS, in: *International Space Station Research and Development Conference*, 2021, pp. 1–24.
- [35] A. Xytkis, L. Papadopoulos, D. Moloney, D. Soudris, S. Yous, Efficient Winograd-based convolution kernel implementation on edge devices, in: *ACM/ESDA/IEEE Design Automation Conference (DAC)*, 2018, pp. 1–6. doi:10.1145/3195970.3196041.
- [36] F. Tsimpourlas, L. Papadopoulos, A. Bartsokas, D. Soudris, A design space exploration framework for convolutional neural networks implemented on edge devices, *IEEE Transactions on Computer-Aided Design of Integrated Circuits and Systems* 37 (11) (2018) 2212–2221. doi:10.1109/TCAD.2018.2857280.
- [37] X. Xu, J. Amaro, S. Caulfield, A. Foremski, G. Falcao, D. Moloney, Convolutional neural network on neural compute stick for voxelized point-clouds classification, in: *International Congress on Image and Signal Processing, BioMedical Engineering and Informatics (CISP-BMEI)*, 2017, pp. 1–7. doi:10.1109/CISP-BMEI.2017.8302078.
- [38] J. Hochstetler, R. Padidela, Q. Chen, Q. Yang, S. Fu, Embedded deep learning for vehicular edge computing, in: *IEEE/ACM Symposium on Edge Computing (SEC)*, 2018, pp. 341–343. doi:10.1109/SEC.2018.00038.
- [39] C. Marantos, N. Karavalakis, V. Leon, V. Tsoutsouras, K. Pekmestzi, D. Soudris, Efficient support vector machines implementation on Intel/Movidius Myriad 2, in: *International Conference on Modern Circuits and Systems Technologies (MOCASST)*, 2018, pp. 1–4. doi:10.1109/MOCASST.2018.8376630.
- [40] L. Puglia, M. Ionică, G. Raiconi, D. Moloney, Passive dense stereo vision on the Myriad2 VPU, in: *IEEE Hot Chips Symposium (HCS)*, 2016, pp. 1–5. doi:10.1109/HOTCHIPS.2016.7936240.
- [41] Intel Corporation, *OpenVINO Toolkit Overview* (2021). URL <https://docs.openvino.ai/2021.2/index.html>
- [42] J. Canny, A computational approach to edge detection, *IEEE Transactions on Pattern Analysis and Machine Intelligence PAMI-8* (6) (1986) 679–698. doi:10.1109/TPAMI.1986.4767851.
- [43] Y. Huang, Y. Bai, R. Li, X. Huang, Research of Canny edge detection algorithm on embedded CPU and GPU heterogeneous systems, in: *International Conference on Natural Computation, Fuzzy Systems and Knowledge Discovery (ICNC-FSKD)*, 2016, pp. 647–651. doi:10.1109/FSKD.2016.7603250.